Available online at www.sciencedirect.com

ScienceDirect

Energy Procedia 114 (2017) 2341 – 2352

Energy Procedia

13th International Conference on Greenhouse Gas Control Technologies, GHGT-13, 14-18 November 2016, Lausanne, Switzerland

Carbon monoliths in adsorption-based post-combustion CO_2 capture

N. Querejeta[a], M.G. Plaza[a], F. Rubiera[a], C.Pevida[a]*, T. Avery[b], S.R. Tennisson[b]

[a]*Instituto Nacional del Carbón, INCAR-CSIC, Apartado 73, Oviedo 33080, Spain*
[b]*MAST Carbon International Ltd., Jay's Close, Basingstoke, Hampshire, RG224BA, UK*

Abstract

The development of adsorption-based technologies for post-combustion CO_2 capture requires finding an adsorbent with adequate equilibrium and transport properties. Structured adsorbents are appealing for fixed-bed TSA processes, because they present lower pressure drop and higher thermal conductivity than conventional adsorbent beds, which facilitates the use of higher flowrates and shorter cycle times, maximizing throughput. In this work, the equilibrium of adsorption of the main flue gas components, CO_2, N_2, O_2 and H_2O over two carbon honeycomb monoliths with different textural development has been measured in a pressure and temperature range of interest for post-combustion CO_2 capture: between 0 °C and 70 °C and up to 120 kPa for CO_2, N_2, and O_2, and between 30 °C and 70 °C up to the corresponding saturation pressure for H_2O. The maximum adsorption capacity and isosteric heat of adsorption follows the order: $H_2O > CO_2 > N_2 \approx O_2$. The carbon monoliths present equilibrium selectivity towards CO_2 and H_2O over N_2 and O_2 at typical flue gas conditions. Moderate activation is preferred to maximize the CO_2 adsorption capacity and selectivity in these conditions. The Toth model was employed to fit the equilibrium data for the adsorption of CO_2, N_2, and O_2 with highly satisfactory results. The adsorption isotherms of H_2O presents the characteristic "s" shape of hydrophobic adsorbents, with low uptakes at low relative pressures, which will facilitate H_2O desorption during cyclic operation. These were fitted using the extended CMMS model, which describes satisfactorily the experimental data in the full relative humidity range. The adsorption kinetics were preliminary evaluated by measuring the rate of mass uptake from a mixture with 10% CO_2 (balance N_2) at 30 °C, 50 °C and 70 °C, and the data were fitted to the linear driving force model to obtain the kinetic rate constants.

Peer-review under responsibility of the organizing committee of GHGT-13.

Keywords: monoliths; adsorption; post-combustion CO_2 capture

* Corresponding author. Tel.: +34-985-119-090; fax: +34-985-297-662.
E-mail address: cpevida@incar.csic.es

Peer-review under responsibility of the organizing committee of GHGT-13.
doi:10.1016/j.egypro.2017.03.1366

Nomenclature

a	channel width (m^{-1})
b_i	affinity constant of *i* component of Toth model (kPa^{-1})
$b_{0,i}$	affinity constant of *i* component of Toth model at the reference temperature T_0 (kPa^{-1})
b_L	Langmuir affinity constant for the interaction of H_2O with the surface functional groups (kPa^{-1})
$b_{L,Tref}$	Langmuir affinity constant at the reference temperature T_{ref} (kPa^{-1})
CMMS	Cooperative Multimolecular Sorption theory
D_e	effective diffusivity ($m^2\ s^{-1}$)
D_s	surface diffusivity ($m^2\ s^{-1}$)
$D_{s,0}$	preexponential factor of the surface diffusivity ($m^2\ s^{-1}$)
E_a	activation energy for surface diffusion (J mol^{-1})
K_0	equilibrium constant for the adsorption of H_2O on the primary site (kPa^{-1})
$K_{0,Tref}$	equilibrium constant for the adsorption of H_2O on the primary site at the reference temperature T_{ref} (kPa^{-1})
K_1	equilibrium constant for the adsorption of H_2O on the side unit of the primary site (kPa^{-1})
$K_{1,Tref}$	equilibrium constant for the adsorption of H_2O on the side unit of the primary site at T_{ref} (kPa^{-1})
k_{LDF}	Linear Driving Force adsorption rate constant (s^{-1})
LDF	Linear Driving Force
MSE	Mean Squared Error
$\bar{n}$	average loading (mmol g^{-1})
n^*	adsorption capacity at equilibrium with the gas phase (mmol g^{-1})
N_A	number of equilibrium data measured at each temperature
N_T	number of temperatures evaluated
n_{calc}	amount adsorbed calculated using the adsorption model (mmol g^{-1})
n_{exp}	amount adsorbed measured experimentally (mmol g^{-1})
n_i	amount adsorbed of *i* component (mmol g^{-1})
n_L	Langmuir saturation capacity of H_2O on the surface functional groups (mmol g^{-1})
$n_{s,i}$	saturation capacity of *i* component of Toth adsorption model (mmol g^{-1})
$n_{\mu s}$	saturation capacity for the adsorption of H_2O in the micropores (mmol g^{-1})
P_i	partial pressure of *i* component in the gas phase (kPa)
PCC	Post-Combustion CO_2 Capture
PSA	Pressure Swing Adsorption
Q_i	isosteric heat of adsorption of of *i* component given by Toth model (J mol^{-1})
q_L	parameter related to the enthalpy of adsorption of H_2O on the surface functional groups (J mol^{-1})
q_0	parameter related to the enthalpy of adsorption of H_2O on the primary sites (J mol^{-1})
q_1	parameter related to the enthalpy of adsorption of H_2O on the side units of the primary sites (J mol^{-1})
R	universal constant of gases
$S_{i/j}$	equilibrium separation factor of species *i* over *j*
T	absolute temperature (K)
t_i	heterogeneity parameter of Toth adsorption model
t_w	wall thickness (m^{-1})
T_0	reference temperature for the adsorption of CO_2, N_2 and O_2 (273 K)
T_{ref}	reference temperature for the adsorption of H_2O (303 K)
TSA	Temperature Swing Adsorption
x_i	molar fraction of *i* component in the adsorbed phase
y_i	molar fraction of *i* component in the gas phase

1. Introduction

The Paris Agreement, adopted in December 2015 at the 21st session of the United Nations Framework Convention on Climate Change (UNFCCC) Conference of the Parties (COP21), aims to strengthen the global response to the threat of climate change by holding the increase in the global average temperature to well below 2 °C above preindustrial levels and pursuing efforts to limit the temperature increase to 1.5 °C [1]. In order to meet such ambitious objective, it is mandatory to substantially mitigate global CO_2 emissions as soon as possible. The agreement, which is yet to be ratified by a sufficient number of countries, is due to enter in legal force in 2020. Given that the energy and industry sectors are still heavily dependent on fossil fuels, the least-cost mitigation scenario makes extensive use of Carbon Capture and Storage (CCS) technologies in the forthcoming decades.

However, the deployment of CCS is hampered by low technical maturity of individual components as well as the CCS infrastructure [2]. Up to date, only one CCS unit is operating at commercial scale in the power sector [3]. This separates the CO_2 present in flue gas by chemical absorption with amine solutions, which is the benchmark technology for post-combustion CO_2 capture (PCC). The main drawback of this option is its high energy intensity due to the need to heat a vast amount of water (nearly 70% by weight) to regenerate the solvent. Alternative separation technologies like membrane and adsorption-based processes seek to reduce the energy and water use of PCC processes. The EU funded HiPerCap project (FP7) aims to develop novel PCC technologies and processes which are environmentally benign and have high potential to lead to breakthroughs in energy consumption and overall cost. A key focus in HiPerCap is to demonstrate the potential of the main separation technologies for PCC (i.e., absorption, adsorption and membranes) by comparing them on a fair basis [4]. HiPerCap is currently evaluating two types of large scale adsorptive separation systems: cyclic multibed processes, in which each adsorbent bed operates alternatively in adsorption or regeneration mode in order to provide continuous feed treatment, and moving bed systems, where the solid and the feed gas circulate countercurrently between an adsorber and a desorber, likewise to absorption systems. In this work, part of the results related to the development of cyclic systems is presented.

The primary requirement to develop an economic adsorption-based separation process is to select a suitable adsorbent, with sufficient capacity, selectivity and lifetime that can be easily regenerated. Carbon adsorbents present equilibrium selectivity towards CO_2 over N_2 and O_2 and have an intrinsic hydrophobic nature that imparts excellent performance in the humid environments that are to be encountered in post-combustion applications [5, 6]. These adsorbents can be easily regenerated, either by heating, which is known as Temperature Swing Adsorption (TSA) or by reducing the pressure, in Pressure Swing Adsorption (PSA) processes. TSA is generally preferred when there is availability of low pressure steam and/or waste heat [7], which is the case of PCC. However, TSA processes present the disadvantage of the time delay imposed by the heating and cooling steps, which *a priori* prevents rapid cycling and increase the adsorbent inventory. The use of structured adsorbents can partially circumvent this difficulty, as they present better heat transfer properties than particulate systems. Carbon monoliths comprise a continuous carbon structure with a thermal conductivity which is nearly two orders of magnitude greater than that of an activated carbon bed. Moreover, the matrix of axial channels in honeycomb monoliths reduces the overall pressure drop of the adsorber compared to their equivalent particulate system [8], which allows the use of higher flowrates, and in turn reduces the diameter of the adsorber and thus the footprint of the capture unit. The improved transport properties of structured adsorbents allow their use in rapid swing adsorption cycles that seek to maximize the separation throughput [9].

In this work the potential of two honeycomb carbon monoliths synthesized from a phenolic resin precursor and activated up to different burn off degrees for PCC adsorption-based cyclic processes is explored. The first step to evaluate the potential of an adsorbent to carry out a certain separation is to study the equilibrium of adsorption for the components that need to be separated in the temperature and pressure range of interest for the intended application. In order to obtain abundant and high quality equilibrium data of interest for PCC, the adsorption isotherms of the main flue gas components, *i.e.*, N_2, CO_2, O_2 and H_2O were measured in commercial adsorption apparatus of manometric type. The collected data allowed assessing the adsorption capacity for the different species and the equilibrium selectivity towards CO_2, but also served as basis to build temperature and pressure dependent adsorption models for the different species. These will be later used to predict multicomponent adsorption equilibrium by making use of the Ideal Adsorbed Solution (IAS) theory [10]. The kinetic of adsorption was also

evaluated by measuring the dynamic adsorption of CO_2 from a mixture with 10% CO_2 and 90% N_2 in a thermogravimetric analyzer in the temperature range of interest for PCC: 30 °C, 50 °C and 70 °C, at atmospheric pressure.

2. Materials and methods

2.1. Materials

In this work, two honeycomb carbon monoliths, 214Jun68 and 214Jun69, that have been activated up to two different burn off degrees, 20% and 50%, are evaluated as candidate adsorbents for PCC. These monoliths were manufactured without binder addition by carbonization and subsequent activation of extruded phenolic resins by MAST Carbon International Ltd. This route provides a unique and detailed control over the structure at the micropore and macropore levels [8].

214Jun68 and 214Jun69 were characterized by N_2 adsorption at -196 °C in a commercial adsorption apparatus TriStar 3000 from Micromeritics. The BET surface area was determined for comparative purposes following the method of Brunauer, Emmett and Teller [11]. The total pore volume was determined by the amount of liquid N_2 adsorbed at a relative pressure of 0.994. Micropore volumes were determined by the Dubinin-Radushkevich method [12] and the average micropore widths by the Stoeckli-Ballerini relation [13].

2.2. Equilibrium of adsorption

The equilibrium of adsorption of pure CO_2, N_2, O_2 and H_2O was evaluated by static measurements carried out using commercial adsorption apparatus. In the case of CO_2, N_2, and O_2, the adsorption and desorption isotherms were measured between 0 kPa and 120 kPa at 0 °C, 30 °C, 50 °C, and 70 °C, using a TriStar 3000 from Micromeritics. The adsorption and desorption isotherms of $H_2O_{(v)}$ at 30 °C, 50 °C, and 70 °C were measured from 0 kPa up to the corresponding saturation pressure, using a sorption analyzer Hydrosorb 1000 HT from Quantachrome. Prior to the adsorption measurements, the samples were outgassed overnight under vacuum at 100 °C. During analysis, the temperature of the sample cell was controlled using a thermostatic bath circulator.

The pure component equilibrium data were fitted to appropriate adsorption models that provide a mathematical description of the equilibrium adsorption capacity as a continuous function of temperature and pressure, most useful for adsorption process design and optimization. The equilibrium data of CO_2, N_2, O_2 were fitted to Toth adsorption model (Equation 1) as this model is relatively simple and provides a satisfactory description of the experimentally measured data. The temperature dependence of the model is given by Equation 2 [14]. Toth parameters, $n_{s,i}$, $b_{0,i}$, t_i and, Q_i were optimized by a nonlinear procedure to give the best fit to the experimental adsorption isotherms, taking the Mean Squared Error (MSE) as the objective function (Equation 3), and using 0 °C (273 K) as the reference temperature.

$$n_i = n_{s,i}\frac{b_i P_i}{(1+(b_i P_i)^t)^{1/t_i}} \tag{1}$$

$$b_i = b_{0,i} exp\left[\frac{Q_i}{RT_0}\left(\frac{T_0}{T}-1\right)\right] \tag{2}$$

$$MSE = \frac{\sum_T\left(\frac{\sum_{i=1}^{N}(n_{exp}-n_{calc})^2}{N_A}\right)\times 100}{N_T} \tag{3}$$

The adsorption isotherms of H_2O were fitted to the composite Langmuir-Ising model proposed by Rutherford [15, 16] (Equations 4-8), which is based on the Cooperative Multimolecular Sorption (CMMS) theory developed by Malahkov and Volkov [17]. Parameters, n_L, $b_{L,Tref}$, q_L, $n_{\mu s}$, $K_{0,Tref}$, q_0, $K_{1,Tref}$, and, q_1 were optimized by a nonlinear procedure to give the best fit to the experimental adsorption isotherms, taking MSE as the objective function

(Equation 3), and using 30 ºC (303 K) as the reference temperature. As the two monoliths under evaluation only differ in their activation extent, the 8 parameters of the composite model were solely optimized for 214Jun68. To fit the data of 214Jun69 only the 5 parameters related to the adsorption in the micropores, $n_{\mu s}$, $K_{0,Tref}$, q_0, $K_{1,Tref}$, and, q_1, were optimized, using the values fitted for 214Jun68 for the Langmuir term of the model. The so optimized parameters are summarized in Table 2.

$$n_{H_2O} = \frac{n_L b_L P_{H_2O}}{1+b_L P_{H_2O}} + \frac{n_{\mu s} K_0 P_{H_2O}}{K_0 P_{H_2O} + {w_{Ising}}^2} \tag{4}$$

$$w_{Ising} = \frac{1}{2}\left[1 - K_1 P_{H_2O} + \sqrt{\left(1 - K_1 P_{H_2O}\right)^2 + 4K_0 P_{H_2O}}\right] \tag{5}$$

$$b_L(T) = b_{L,T_{ref}} exp\left[\frac{q_L}{RT_{ref}}\left(\frac{T_{ref}}{T} - 1\right)\right] \tag{6}$$

$$K_0(T) = K_{0,T_{ref}} exp\left[\frac{q_0}{RT_{ref}}\left(\frac{T_{ref}}{T} - 1\right)\right] \tag{7}$$

$$K_1(T) = K_{1,T_{ref}} exp\left[\frac{q_1}{RT_{ref}}\left(\frac{T_{ref}}{T} - 1\right)\right] \tag{8}$$

The isosteric heat of adsorption of H_2O, CO_2, N_2 and O_2, was estimated from the experimental adsorption isotherms using the slope of the isosteres with linear regression coefficient greater than 0.999.

2.3. Kinetics of adsorption

The kinetics of adsorption of the samples under study were preliminary evaluated by measuring the dynamic mass uptake from a binary mixture consisting in 10% CO_2 (balance N_2) using a thermogravimetric analyzer from Mettler Toledo following the procedure detailed in [18] at three different temperatures: 30 °C, 50 °C, and 70 °C. The experimental uptake curves were fitted to a linear driving force model [19] (Equation 9) following the procedure detailed in [18] to extract the kinetic rate constants.

$$\frac{d\bar{n}}{dt} = k_{LDF}(n^* - \bar{n}) \tag{9}$$

The linear driving force coefficient for a honeycomb monolith with square channels can be written as a function of the diffusivity and the geometrical characteristics of the monolith as given by Equation 10 [20].

$$k_{LDF} = \frac{4D_e}{\left\{\left(\frac{r_o}{r_i}-1\right)({r_o}^2-{r_i}^2) - \left(\frac{1}{r_i(r_o-r_i)}\right)\left[\frac{1}{2}({r_o}^4-{r_i}^4) - \frac{4r_o}{3}({r_o}^3-{r_i}^3) + {r_o}^2({r_o}^2-{r_i}^2)\right]\right\}} \tag{10}$$

where: $r_i = \frac{2a}{\pi}$ and $r_o = \sqrt{\frac{4t_w}{\pi}(t_w + a) + {r_i}^2}$

3. Results and discussion

3.1. Characterization

The textural characterization of 214Jun68 and 214Jun69 is summarized in Table 1. Both carbons are essentially microporous. 214Jun69 presents nearly twice the micropore volume of 214Jun68, but also a wider average micropore size than 214Jun68 due to its higher activation degree.

Table 1. Textural characterization of the carbon monoliths 214Jun68 and 214Jun69 obtained from the N_2 adsorption isotherms at 77 K

	S_{BET} (m^2 g^{-1})	V_p (cm^3 g^{-1})	V_0 (cm^3 g^{-1})	L_0 (nm)
214Jun68	1089	0.38	0.38	0.59
214Jun69	1818	0.73	0.71	1.11

3.2. Equilibrium of adsorption

Fig 1 shows the CO_2 adsorption isotherms of the two monoliths under study at 0 °C, 30 °C, 50 °C and 70 °C up to 120 kPa. The CO_2 adsorption capacity of 214Jun68 and 214Jun69 is greater than that of a likewise honeycomb carbon monolith that presented lower micropore volume [21].

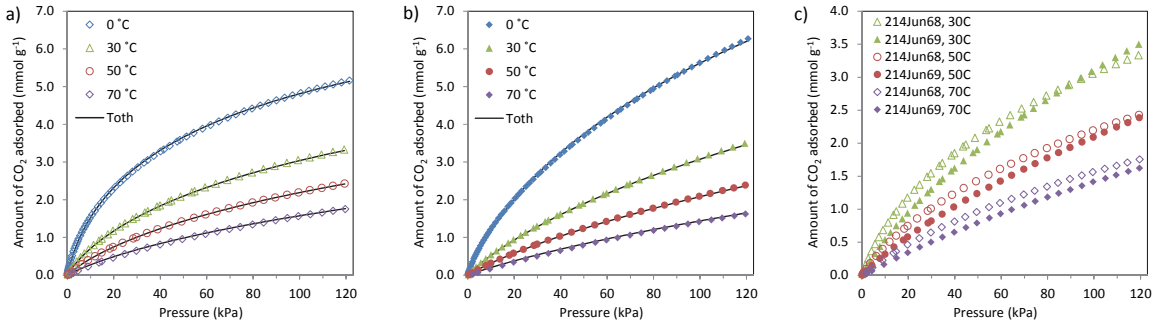

Fig. 1. Adsorption isotherms of CO_2 at 0 °C, 30 °C, 50 °C and 70 °C up to 120 kPa on: a) 214Jun68 and b) 214Jun69; c) comparison of the CO_2 adsorption isotherms at 30 °C, 50 °C and 70 °C of 214Jun68 and 214Jun69.

Too frequently, the adsorption capacity at 0 °C and 101 kPa has been taken as a decision parameter to evaluate the potential of adsorbents for their application in PCC. As can be seen from Fig. 1, the CO_2 adsorption capacity at 0 °C and 101 kPa of 214Jun69 is greater than that of 214Jun68. However, in Fig 1c it can be seen that for CO_2 partial pressures below 80 kPa and in the temperature range of interest for PCC, 30-70 °C, the adsorption capacity of 214Jun68, which is the monolith with lower activation extent, is greater than that of 214Jun69, despite the greater surface area and pore volume of the latter. This is because as activation proceeds, the narrow micropores, which are responsible for the adsorption of CO_2 due to the overlapping adsorption potential of opposite walls, are widened, being less effective to "trap" the CO_2 in PCC conditions. The adsorption capacity of 214Jun68 at 15 kPa at 30 °C is 1.0 mmol g^{-1}, which is also higher than that reported for an ammonia modified activated carbon monolith synthesized from African Palm stone by chemical activation [22]. The goodness of fit of Toth model is shown in Figs. 1a and 1b, where symbols represent the experimental data and the solid lines the model prediction.

Fig. 2 shows the N_2 adsorption isotherms of the monoliths under study at 0 °C, 30 °C, 50 °C and 70 °C up to 120 kPa. Comparing Fig 1 and Fig. 2 it is clear that the equilibrium adsorption capacity towards N_2 on the carbon monoliths is substantially lower than that presented for CO_2, which means that the carbons present CO_2 over N_2 equilibrium selectivity, and that the separation N_2/CO_2 is feasible. Toth adsorption model reproduces satisfactorily

the experimental data for N_2 adsorption, as shown in Fig. 2a and Fig. 2b. Fig. 2c compares the N_2 adsorption isotherms for the samples evaluated. 214Jun68 presents slightly higher adsorption capacity than 214Jun69 at 30 °C, although the difference grows smaller as temperature increases.

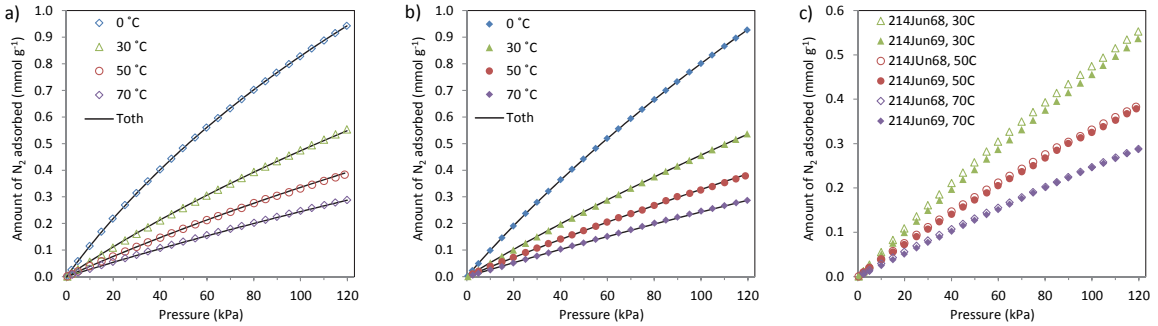

Fig. 2. Adsorption isotherms of N_2 at 0 °C, 30 °C, 50 °C and 70 °C up to 120 kPa on: a) 214Jun68 and b) 214Jun69; c) comparison of the N_2 adsorption isotherms at 30 °C, 50 °C and 70 °C of 214Jun68 and 214Jun69.

Fig. 3 shows the adsorption isotherms of O_2 over the monoliths under study at 0 °C, 30 °C, 50 °C and 70 °C up to 120 kPa. As can be seen from the figure, Toth adsorption model, represented by the solid lines, reproduces satisfactorily the experimental data, represented by the symbols. Fig. 3c shows that 214Jun68 presents slightly higher O_2 adsorption capacity than 214Jun69 in the whole temperature and pressure range evaluated.

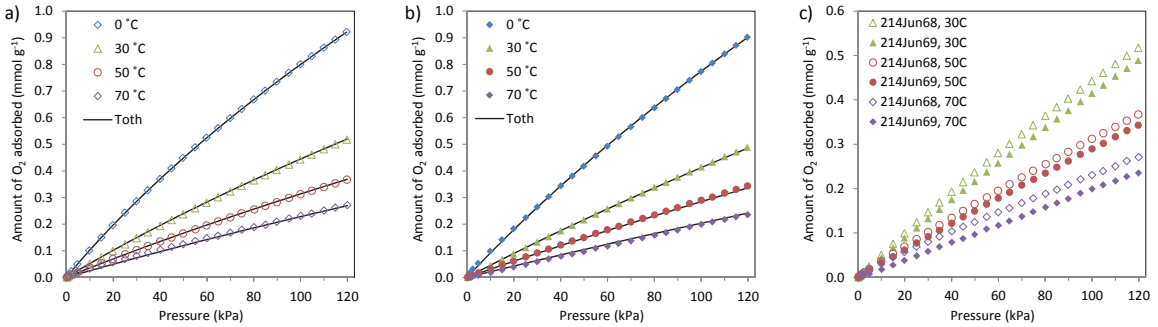

Fig. 3. Adsorption isotherms of O_2 at 0 °C, 30 °C, 50 °C and 70 °C up to 120 kPa on: a) 214Jun68 and b) 214Jun69; c) comparison of the O_2 adsorption isotherms at 30 °C, 50 °C and 70 °C of 214Jun68 and 214Jun69.

Table 2 shows the optimal Toth parameters for the adsorption of CO_2, N_2 and O_2 on the carbon monoliths 214Jun68 and 214Jun69.

Table 2. Optimal Toth parameters for the adsorption of CO_2, N_2 and O_2 on carbon monoliths 214Jun68 and 214Jun69

	214Jun68			214Jun69		
	CO_2	N_2	O_2	CO_2	N_2	O_2
n_s (mmol g^{-1})	11.09	4.16	7.73	27.96	8.96	8.54
b_0 (kPa^{-1})	0.0324	0.0030	0.0014	0.0069	0.0012	0.0011
t	0.520	0.802	0.704	0.491	0.718	0.783
Q (J mol^{-1})	25147	16534	16159	22925	15091	16457

As expected, the heterogeneity parameter that presents greater deviation from unity is that of CO_2, which is in good agreement with the higher value of the parameter *Q*, which represents the isosteric heat of adsorption given by the model.

Fig. 4 shows the adsorption isotherms of H_2O at 30 °C, 50 °C and 70 °C on carbon monoliths 214Jun68 and 214Jun69. The isotherms present the characteristic "s" shape for H_2O adsorption on hydrophobic carbon adsorbents, with negligible uptake at low relative pressures and an asymptotic adsorption capacity at high relative humidity. This equilibrium behavior facilitates the desorption of water vapor compared to adsorption isotherms of Type I or Type II, characteristic of hydrophilic adsorbents, which present high adsorption capacity from very low relative pressures. The large H_2O uptake that takes place at intermediate relative pressures corresponds to the adsorption in the micropores [23]. 214Jun69 presents nearly twice the maximum adsorption capacity of 214Jun68 due to its higher micropore volume. It must be borne in mind that low adsorption capacity towards H_2O is desired for adsorbents to be used in PCC, as water adsorption will reduce the working capacity of CO_2 [24]. Again, these results point out that the best adsorbent is not necessarily that with the highest pore volume.

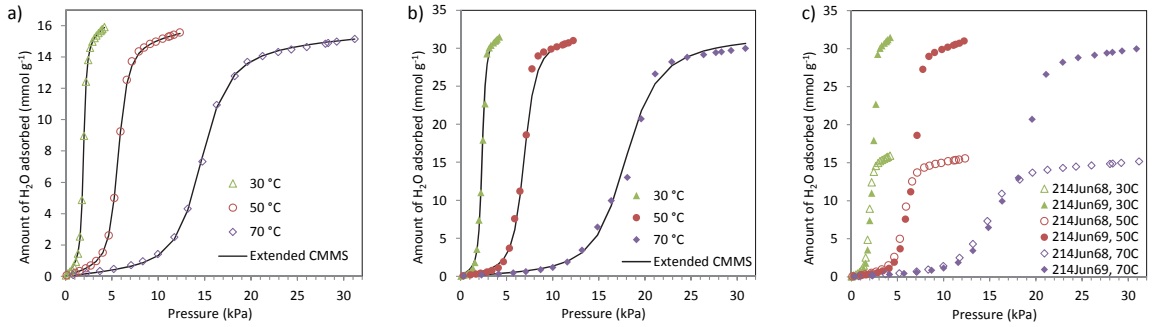

Fig. 4. Adsorption isotherms of H_2O at 30 °C, 50 °C and 70 °C up to the corresponding saturation pressure on: a) 214Jun68 and b) 214Jun69; c) comparison of the H_2O adsorption isotherms of 214Jun68 and 214Jun69.

Table 3. Optimal parameters of the extended CMMS model for the adsorption of H_2O on 214Jun68 and 214Jun69

	214Jun68	214Jun69
n_L (mmol g^{-1})	7.5929	7.5929
$b_{L,\,30\,°C}$ (kPa^{-1})	0.0941	0.0941
q_L (J mol^{-1})	53657	53657
$n_{\mu s}$ (mmol g^{-1})	13.8822	30.0827
$K_{0,30\,°C}$ (kPa^{-1})	0.0037	0.0034
q_0 (J mol^{-1})	35740	38533
$K_{1,30\,°C}$ (kPa^{-1})	0.5126	0.4241
q_1 (J mol^{-1})	43814	44009

The goodness of fit of the extended CMMS theory to the experimental data can be seen in Figs. 4a and 4b, where the model is represented by solid lines and the experimental data by symbols. The extended CMMS model presents the advantage of its relative simplicity, which allows the introduction of the temperature and pressure dependent equilibrium relation in the mathematical model of the adsorption process, which can be used for process design and optimization [24]. Table 3 summarizes the parameters of the extended CMMS model. The values of K_1 and q_1 are greater than those of K_0 and q_0, respectively, because the adsorption of H_2O on the carbon is enhanced by H-bonding when there are H_2O molecules adsorbed nearby. The value obtained for q_1 is close to the heat of condensation of H_2O. Note that the saturation capacity in the micropores, $n_{\mu s}$, of 214Jun69 is twice that of 214Jun68.

The isosteric heat of adsorption of H_2O, CO_2, N_2 and O_2 on 214Jun68 and 214Jun69 is represented in Figs. 5a and 5b, respectively, *versus* the adsorbed amount of each species. This follows the order: $H_2O > CO_2 > N_2 \approx O_2$ with average values that are in good agreement with the values given by the adsorption models. The same trend is observed for the equilibrium adsorption capacity of the main flue gas components on the carbon monoliths at a given temperature and partial pressure. See for example in Fig. 5c the comparison of the adsorption isotherms at 50 °C on 214Jun68.

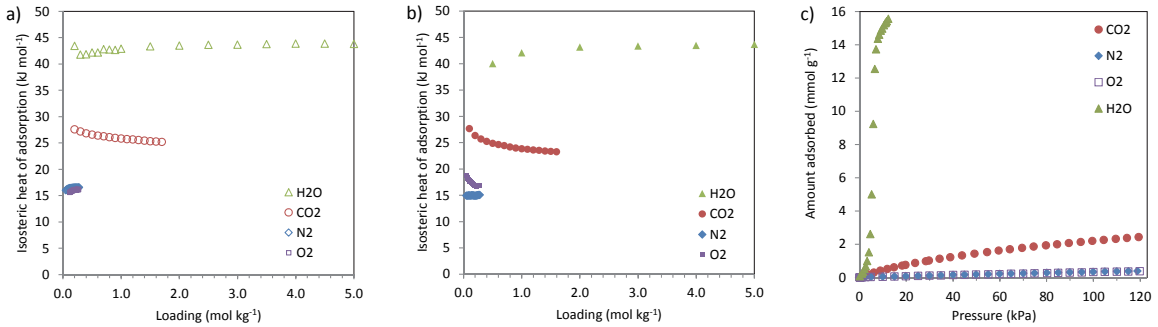

Fig. 5. Isosteric heat of adsorption of H_2O, CO_2, N_2 and O_2 on: a) 214Jun68 and b) 214Jun69; c) comparison of the equilibrium adsorption isotherms of H_2O, CO_2, N_2 and O_2 on 214Jun68 at 50 °C.

The equilibrium selectivity of an adsorbent for a specific separation is generally assessed in a first approximation using the equilibrium separation factor, which is defined by Equation 11:

$$S_{i/j} = \frac{x_{i/x_j}}{y_{i/y_j}} \tag{11}$$

Using the previous definition, we have estimated the equilibrium separation factor for a standard coal-fired flue gas after desulphurization, which is at 47 °C and at a pressure of 105 kPa, and presents a composition by volume of 71.694% N_2, 3.687% O_2, 13.597% CO_2 and 10.16% H_2O (balance: Ar and trace amounts of SO_2) based on the pure component adsorption models. Results for 214Jun68 and 214 Jun69 are shown in Table 4. Note that the values given in the table have been calculated using the pure component models; any multicomponent model that considers competitive adsorption will give higher values for the separation factor. Both monoliths present equilibrium selectivity for CO_2 and H_2O over N_2 and O_2, and for H_2O over CO_2, which is detrimental, as the adsorption of H_2O will reduce the working capacity of CO_2. Nevertheless, the selectivity of H_2O over CO_2 of 214Jun68 is relatively low compared to that of 214Jun69 or to other adsorbents. Moreover, the CO_2 selectivity over N_2 and O_2 is higher for 214Jun68, which points out that adsorbents with moderate texture developments can be more adequate for PCC applications.

Table 4. Separation factor for a standard coal-fired flue gas after wet desulphurization

	214Jun68	214Jun69
$S_{CO2/N2}$	12	9
$S_{CO2/O2}$	21	10
$S_{H2O/CO2}$	34	89
$S_{H2O/N2}$	400	831
$S_{H2O/O2}$	704	857

3.3. Kinetics of adsorption

Figs. 6a and 6b show the dynamic mass uptake of samples 214Jun68 and 214Jun69 (in equilibrium with flowing N_2 at t=0) when the feed gas is switched from 100% N_2 to a binary mixture with 10% CO_2 and 90% N_2 at constant temperature and atmospheric pressure. The mass increase observed in the figures is due to the adsorption of CO_2 from the gas mixture. This has been represented as fractional uptake versus time to facilitate comparison between the different adsorption temperatures. From the figure, it can be seen that as temperature increases, the curves become steeper. The rate of adsorption is satisfactorily described by the LDF model as shown in Fig. 6a and Fig. 6b, where the symbols represent the experimental data and the solid lines the optimized LDF model. The optimal values of the adsorption rate constant at the three temperatures evaluated can be found in Table 5. These are slightly higher for 214Jun68. For both samples, the values of the LDF constants increase with temperature. The rate limiting mechanism is most likely surface diffusion, and surface diffusivity is known to depend exponentially with temperature according to Equation 12 [14].

$$D_s = D_{s0} exp\left(-\frac{E_a}{RT}\right) \tag{12}$$

The effective diffusivity, D_e, was calculated from the optimal values of k_{LDF} using Equation 10. The effective diffusivity of 214Jun68 and 214Jun69 at 30 °C is $4.0 \cdot 10^{-9}$ and $3.6 \cdot 10^{-9}$ m^2 s^{-1}, respectively, which are typical values for physical adsorption systems. Plotting *ln* D_e against *1/T* for each sample, two straight lines with squared regression coefficients of 0.99 were obtained (see Fig. 6c), from which slopes the activation energies (E_a) for surface diffusion were extracted, and from their intercepts, the preexponential factors (D_{s0}). The values obtained are shown in Table 5. The activation energy for surface diffusion is nearly half the value of the isosteric heat of adsorption of CO_2, which is to be expected for physisorption processes [25]. The values obtained are in good agreement with the value reported for the surface diffusivity of a different honeycomb carbon monolith at 298 K [26]. However, higher values for E_a and lower values of D_s have also been reported for other carbon honeycomb monoliths [21].

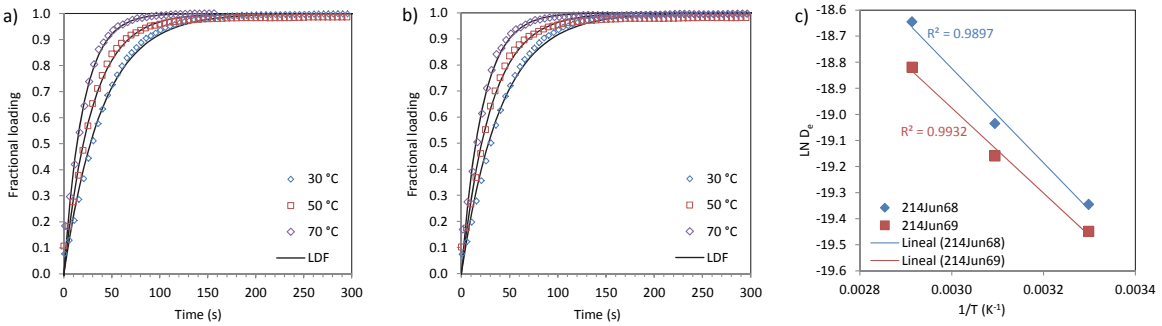

Fig. 6. Dynamic mass uptake at 30 °C, 50 °C and 70 °C from a mixture with 10% CO_2 (balance N_2) at atmospheric pressure of: a) 214Jun68 and b) 214Jun69; c) plot of lnD_e *versus 1/T* for samples 214Jun68 and 214Jun69.

Table 5. Optimal LDF adsorption rate constants obtained for samples 214Jun68 and 214Jun69 and estimated preexponential factor and activation energy for surface diffusion

	214Jun68	214Jun69
$k_{LDF,\,30\,°C}$ (s^{-1})	0.025	0.025
$k_{LDF,\,50\,°C}$ (s^{-1})	0.034	0.033
$k_{LDF,\,70\,°C}$ (s^{-1})	0.051	0.046
D_{s0} $(m^2\,s^{-1})$	$1.5 \cdot 10^{-6}$	$7.7 \cdot 10^{-7}$
E_a $(kJmol^{-1})$	15.073	13.574

4. Conclusions

The potential of two resin-based activated carbon honeycomb monoliths for their use in adsorption-based post-combustion CO_2 capture processes was explored. Although the monolith with greater activation extent (214Jun69) presents higher micropore volume, the lesser activated monolith (214Jun68) presents a narrower average micropore width, which is relevant for the adsorption of CO_2 under post-combustion conditions.

The equilibrium of adsorption of the main flue gas components, N_2, CO_2, O_2 and H_2O was studied in a wide temperature and pressure range of interest for the intended application: between 0 °C and 70 °C and up to 120 kPa for N_2, CO_2, O_2 and between 30 °C and 70 °C and up to the saturation pressure for H_2O. The maximum adsorption capacity follows the same order as the isosteric heat of adsorption: $H_2O > CO_2 > N_2 \approx O_2$. The CO_2 adsorption capacity at partial pressures typical of flue gases is higher for 214Jun68 due to its narrower porosity. Both samples present equilibrium selectivity for CO_2 over N_2 and O_2, although the selectivity of 214Jun68 towards CO_2 is superior. The H_2O equilibrium capacity of 214Jun69 at the high relative humidity that is to be encountered after a wet desulphurization unit, is twice that of 214Jun68. Both monoliths present equilibrium selectivity for H_2O over CO_2, albeit this is lower for 214Jun68. From the equilibrium point of view, it is clear that the moderately activated carbon monolith presents greater potential to be used in PCC applications. Obviously, a lower activation degree is also beneficial for manufacturers as it increases substantially the product yield but also reduces the length of the activation treatment reducing the manufacturing cost.

Adsorption models provide convenient equations that relate the equilibrium adsorption capacity to the temperature and partial pressure of the gas phase. The equilibrium of adsorption of N_2, CO_2, and O_2 in the temperature and pressure range evaluated is satisfactorily described by the relatively simple Toth adsorption model, and the equilibrium of adsorption of H_2O is adequately described by the extended CMMS theory. These models can be used to predict adsorption equilibrium of gas mixtures making use of the IAS theory.

From the kinetic point of view, both carbons present fast adsorption of CO_2 from a N_2/CO_2 mixture, although 214Jun68 presents slightly higher adsorption rate than 214Jun69. The dynamic adsorption can be adequately described by the linear driving force approximation. The adsorption rate constants increase exponentially with temperature, which points out a surface diffusion rate limiting mechanism in the conditions evaluated with activation energies of 13.6 and 15.1 kJ $mol^{-1}$for 214Jun69 and 214Jun68, respectively.

Acknowledgements

Work carried out with financial support from the HiPerCap Project of the European Union 7th Framework Programme FP7 (2007-2013; Grant Agreement number: 60855). N.Q. acknowledges a fellowship from the Gobierno del Principado de Asturias (Programa Severo Ochoa).

References

[1] COP, *Paris Agreement*. United Nations Framework Convention on Climate Change (UNFCCC): FCCC/CP/2015/10/Add.1; 2015.

[2] Stigson P, Hansson A, Lind M. Obstacles for CCS deployment: an analysis of discrepancies of perceptions. *Mitig Adapt Strateg Glob Change* 2012; 17: 601-19.

[3] Stéphenne K. Start-up of world's first commercial post-combustion coal fired CCS project: contribution of Shell Cansolv to SaskPower Boundary Dam ICCS project. *Energy Procedia* 2014; 63: 6106-10.

[4] Kvamsdal HM, Kim I, Van Os P, Pevida C, Hägg M-B, Brown J, Robinson L, Feron P. HiPerCap: A New FP7 Project for Development and Assessment of Novel and Emerging Post-combustion CO_2 Capture Technologies. *Energy Procedia* 2014; 63: 6166-72.

[5] Plaza MG, González AS, Rubiera F, Pevida C. Water vapour adsorption by a coffee-based microporous carbon: effect on CO_2 capture. *J Chem Technol Biotechnol* 2015; 90: 1592-600.

[6] Plaza MG, González AS, Pevida C, Rubiera F. Influence of water vapor on CO_2 adsorption using a biomass-based carbon. *Ind Eng Chem Res* 2014; 53: 15488−99.

[7] Ruthven DM. Principles of adsorption and adsorption processes. New York: John Wiley and Sons; 1984.

[8] Crittenden B, Patton A, Jouin C, Perera S, Tennison S, Echevarria J. Carbon monoliths: a comparison with granular materials. *Adsorption* 2005; 11: 537-41.
[9] Hedin N, Andersson L, Bergström L, Yan J. Adsorbents for the post-combustion capture of CO_2 using rapid temperature swing or vacuum swing adsorption. *Appl Energy* 2013; 104: 418-33.
[10] Myers AL, Prausnitz JM. Thermodynamics of mixed-gas adsorption. *AIChE J* 1965; 11: 121-7.
[11] Brunauer S, Emmett PH, Teller E. Adsorption of gases in multimolecular layers. *J Am Chem Soc* 1938; 60: 309-19.
[12] Dubinin MM, Stoeckli HF. Homogeneous and heterogeneous micropore structures in carbonaceous adsorbents. *J Colloid Interface Sci* 1980; 75: 34-42.
[13] Stoeckli F, Ballerini L. Evolution of microporosity during activation of carbon. *Fuel* 1991; 70: 557-9.
[14] Do DD. Adsorption analysis: equilibria and kinetics. Yang RT, Ed. Series on Chemical Engineering Singapore: Imperial College Press; 1998.
[15] Rutherford SW. Application of cooperative multimolecular sorption theory for characterization of water adsorption equilibrium in carbon. *Carbon* 2003; 41: 622-5.
[16] Rutherford SW. Modeling water adsorption in carbon micropores: study of water in carbon molecular sieves. *Langmuir* 2006; 22: 702-8.
[17] Malakhov AO, Volkov VV. Cooperative multimolecular sorption equation: Application to an alcohol-poly(1-trimethylsilyl-1-propyne) system. *Polym Sci, Ser A* 2000; 40: 1120-6.
[18] Plaza MG, Durán I, Rubiera F, Pevida C. CO_2 adsorbent pellets produced from pine sawdust: Effect of coal tar pitch addition. *Appl Energy* 2015; 144: 182-92.
[19] Glueckauf E, Coates JI. 241. Theory of chromatography. Part IV. The influence of incomplete equilibrium on the front boundary of chromatograms and on the effectiveness of separation. *J Chem Soc* 1947; 0: 1315-21.
[20] Patton A, Crittenden BD, Perera SP. Use of the linear driving force approximation to guide the design of monolithic adsorbents. *Chemical Engineering Research and Design* 2004; 82: 999-1009.
[21] Ribeiro RP, Sauer TP, Lopes FV, Moreira RF, Grande CA, Rodrigues AE. Adsorption of CO_2, CH_4, and N_2 in activated carbon honeycomb monolith. *J Chem Eng Data* 2008; 53: 2311-7.
[22] Vargas DP, Balsamo M, Giraldo L, Erto A, Lancia A, Moreno-Piraján JC. Equilibrium and dynamic CO_2 adsorption on activated carbon honeycomb monoliths. *Ind Eng Chem Res* 2016; 55: 7898-905.
[23] Do DD, Junpirom S, Do HD. A new adsorption–desorption model for water adsorption in activated carbon. *Carbon* 2009; 47: 1466-73.
[24] Plaza MG, Durán I, Querejeta N, Rubiera F, Pevida C. Experimental and simulation study of adsorption in postcombustion conditions using a microporous biochar 2. H_2O, CO_2, and N_2 adsorption. *Ind Eng Chem Res* 2016.
[25] Sladek KJ, Gilliland ER, Baddour RF. Diffusion on surfaces II. Correlation of diffusivities of physically and chemically adsorbed species. *Ind Eng Chem Fundam* 1974; 13: 100-5.
[26] Ahn H, Brandani S. Dynamics of carbon dioxide breakthrough in a carbon monolith over a wide concentration range. *Adsorption* 2005; 11: 473-7.